

Platinum Acetate Blue: Synthesis and Characterization

Natalia V. Cherkashina,[†] Dmitry I. Kochubey,[‡] Vladislav V. Kanazhevskiy,[‡] Vladimir I. Zaikovskii,^{‡,§} Vladimir K. Ivanov,[†] Alexander A. Markov,[†] Alla P. Klyagina,[†] Zhanna V. Dobrokhotova,[†] Natalia Yu. Kozitsyna,[†] Igor B. Baranovsky,[†] Olga G. Ellert,[†] Nikolai N. Efimov,[†] Sergei E. Nefedov,[†] Vladimir M. Novotortsev,[†] Michael N. Vargaftik,^{*,†} and Ilya I. Moiseev[†]

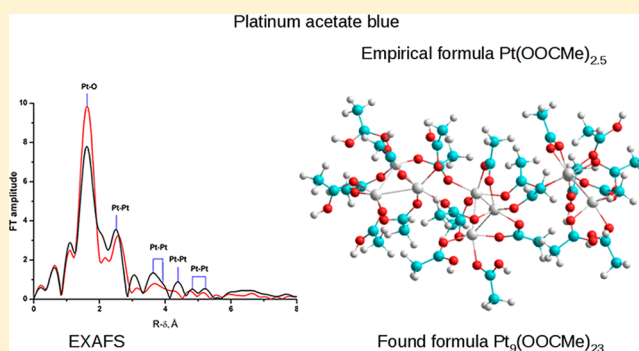
[†]N.S. Kurnakov Institute of General and Inorganic Chemistry, Russian Academy of Sciences, 119991, Moscow, Russian Federation

[‡]G.K. Boreskov Institute of Catalysis, Siberian Branch of Russian Academy of Sciences, 630090, Novosibirsk, Russian Federation

[§]Novosibirsk State University, 630090, Novosibirsk, Russian Federation

Supporting Information

ABSTRACT: Platinum acetate blue (PAB) of the empirical formula $\text{Pt}(\text{OOCMe})_{2.5 \pm 0.25}$, a byproduct in the synthesis of crystalline platinum(II) acetate $\text{Pt}_4(\text{OOCMe})_8$, is an X-ray amorphous substance containing platinum in the oxidation state between (II) and (III). Typical PAB samples were studied with X-ray diffraction, differential thermal analysis–thermogravimetric, extended X-ray absorption fine structure, scanning electron microscopy, transmission electron microscopy, magnetochemistry, and combined quantum chemical density functional theory–molecular mechanics modeling to reveal the main structural features of the PAB molecular building blocks. The applicability of PAB to the synthesis of platinum complexes was demonstrated by the preparation of the new homo- and heteronuclear complexes $\text{Pt}^{\text{II}}(\text{dipy})(\text{OOCMe})_2$ (1), $\text{Pt}^{\text{II}}(\mu\text{-OOCMe})_4\text{Co}^{\text{II}}(\text{OH}_2)$ (2), and $\text{Pt}^{\text{III}}_2(\text{OOCMe})_4(\text{O}_3\text{SPhMe})_2$ (3) with the use of PAB as starting material.



INTRODUCTION

Crystalline platinum(II) acetate $\text{Pt}_4(\text{OOCMe})_8$, a promising starting material for the synthesis of platinum complexes and nanomaterials, is infrequently used in industrial and research-scale practices (see examples in refs 1–3) because of its limited accessibility. Although the crystal and electronic structure of $\text{Pt}_4(\text{OOCMe})_8$ was established long ago,^{4,5} the known preparation methods^{6–12} are poorly reproducible, affording platinum(II) acetate in insufficient yield, along with a greater amount of a dark-blue to brown byproduct, a noncrystalline platinum blue containing Pt in the oxidation states between (II) and (III).

The first platinum blue, a dark blue substance reported as Platin Blau of the empirical formula $\text{Pt}(\text{CH}_3\text{CONH})_2 \times \text{H}_2\text{O}$, was obtained by K.A. Hofmann and G. Bugge as early as 1908 by the reaction of *cis*- $\text{PtCl}_2(\text{CH}_3\text{CN})_2$ with Ag_2SO_4 .¹³ To the best of our knowledge, none of the noncrystalline platinum blues were studied with physicochemical methods. Meanwhile, a number of antitumor active crystalline platinum blues stabilized with N-donor ligands have been synthesized and structurally characterized with X-ray crystallography (see, e.g., refs 14–23).

This work aims to shed some light on the chemical nature of the noncrystalline mixed-valent platinum acetate blue (PAB). For this purpose, we prepared representative samples of PAB of

the empirical formula $\text{Pt}(\text{OOCMe})_{2.5 \pm 0.25}$ and studied them with X-ray diffraction (XRD), differential thermal analysis–thermogravimetric (DTA-TG), extended X-ray absorption fine structure (EXAFS), scanning electron microscopy (SEM), transmission electron microscopy (TEM), magnetic susceptibility measurements, and quantum chemical density functional theory–molecular mechanics (DFT–MM+) modeling to reveal the most probable equilibrium geometry of the PAB structural fragments corresponding to the experimental data. Also we found that PAB can be used as starting material for the synthesis of platinum carboxylate complexes instead of the difficult-to-access and less reactive crystalline $\text{Pt}_4(\text{OOCMe})_8$.

Earlier we used PAB as starting material in the synthesis of the platinum(II) mixed-ligand complex $\text{Pt}^{\text{II}}_4(\text{OOCMe})_4(\text{OOC}^t\text{Bu})_4$ and platinum(III) lantern complex $\text{Pt}^{\text{III}}_2(\text{OOCMe})_4(\text{O}_3\text{SMe})_2$.^{24,25} In this work, we prepared with the use of PAB the new platinum homo- and heteronuclear carboxylate complexes $\text{Pt}^{\text{II}}(\text{dipy})(\text{OOCMe})_2$ (1), $\text{Pt}^{\text{II}}(\mu\text{-OOCMe})_4\text{Co}^{\text{II}}(\text{OH}_2)$ (2), and $\text{Pt}^{\text{III}}_2(\text{OOCMe})_4(\text{O}_3\text{SPhMe})_2$ (3) and established their structure by single-crystal X-ray diffraction.

Received: April 23, 2014

Published: August 7, 2014

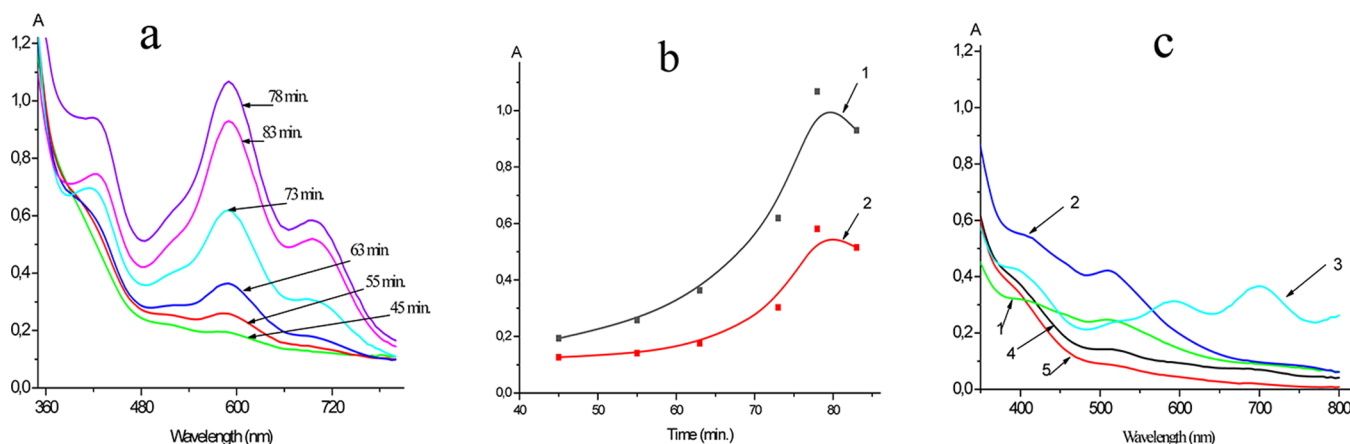


Figure 1. UV-vis absorption spectra: (a) time course of the spectrum of the reaction solution (2.66 mmol of $\text{K}_2\text{Pt}(\text{OH})_6$, 1.96 mmol of formic acid, 50 mL of acetic acid, 95 °C); (b) time profile of the absorption values at 590 nm (curve 1) and 700 nm (curve 2) of the reaction solution; (c) 3.0×10^{-4} mol/L solutions in acetic acid of different PAB samples isolated from the reaction solution: 1 – $\text{Pt}(\text{OOCMe})_2$; 2 – $\text{Pt}(\text{OOCMe})_{2.25}$; 3 – $\text{Pt}(\text{OOCMe})_{2.5}$; 4 – $\text{Pt}(\text{OOCMe})_{2.75}$; 5 – $\text{Pt}(\text{OOCMe})_3$.

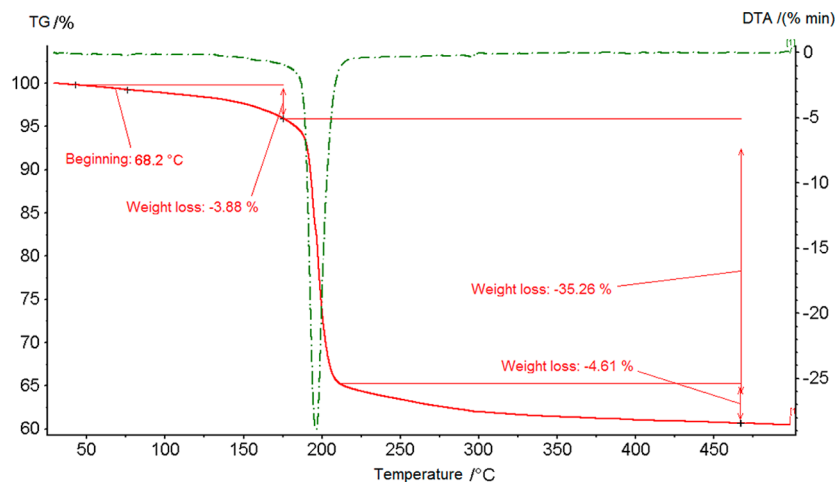


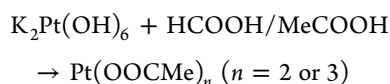
Figure 2. TG-DTA data for thermal decomposition of PAB 1 of the empirical formula $\text{Pt}(\text{OOCMe})_{2.5}$ (Ar flow, heating rate 10 deg/min).

RESULTS AND DISCUSSION

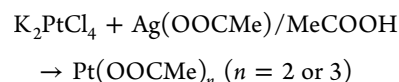
Two main approaches to the synthesis of crystalline platinum(II) acetate are known: (1) reduction of Pt^{IV} chloro/nitro complexes with formic acid in HNO_3 -acetic acid medium^{6,7} or $\text{K}_2[\text{Pt}(\text{OH})_6]$ in glacial acetic acid;⁸ (2) metathesis of platinum(II) chloro or bromo complex with silver(I) acetate.⁹ Repeated attempts to prepare crystalline platinum(II) acetate by both methods met with little success (see, e.g., refs 8, 10–12), resulting in a low yield of the target product, along with a greater amount of a dark-blue to brown noncrystalline platinum acetate blues containing Pt in the oxidation states between (II) and (III). The metathetical reaction is accompanied by the partial oxidation of Pt^{II} with Ag^{I} : $\text{Pt}^{2+} + \text{Ag}^+ = \text{Pt}^{3+} + \text{Ag}^0$.

In this work we used both synthetic approaches for the preparation of PAB:

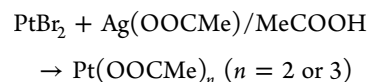
1. Partial reduction of platinum(IV) with formic acid in glacial acetic acid (PAB 1, Protocol 1):



2. Metathesis of platinum(II) chloride with silver acetate in glacial acetic acid accompanied by partial oxidation of platinum(II) (PAB 2, Protocol 2):



3. Metathesis of platinum(II) bromide with silver acetate in glacial acetic acid accompanied by partial oxidation of platinum(II) (PAB 3, Protocol 3):



It was unclear whether the noncrystalline solid prepared by these methods is a uniform material or a conglomerate of different species. Hence, it was of interest to find out the main structural units of the representative PAB samples. For this purpose, we prepared the most reproducible PAB samples, mostly PAB 1 of the empirical formula $\text{Pt}(\text{OOCMe})_{2.5}$, and studied them with UV-vis, XRD, DTA-TG, SEM, high-resolution electron microscopy (HREM), EXAFS, and magnetic susceptibility measurements. Combined DFT quan-

tum chemical and molecular mechanics (MM+) were carried out to fit the experimental data.

UV-visible Spectra. The time course of the UV-vis absorption spectra of the reaction solution during the synthesis according to Protocol 1 (Figure 1a,b) showed the first-order accumulation of the main reaction product with the absorption maxima at 590 and 700 nm until ~75 min of reaction time. The wavelengths of these peaks reasonably agree with those for the solution in acetic acid of the final reaction product of the empirical formula $\text{Pt}(\text{OOCMe})_{2.5}$ prepared according to Protocol 1. When the reaction time was varied within 10 to 120 min, the isolated final reaction product varied in composition from $\text{Pt}(\text{OOCMe})_2$ to $\text{Pt}(\text{OOCMe})_3$ (Figure 1c).

The samples other than $\text{Pt}(\text{OOCMe})_{2.5}$ revealed no absorption maxima at these wavelengths. Hence, we used the PAB samples with the reproducible empirical formula of $\text{Pt}(\text{OOCMe})_{2.5}$, prepared according to Protocol 1 in the following physicochemical studies.

Thermogravimetric Analysis–Differential Thermal Analysis. These data (Figure 2) gave some evidence of the homogeneity of the PAB main body: it thermally decomposes rather sharply at 190 °C, and the total weight loss (43.75%) reasonably agrees with the total ligand percentage in the PAB sample (43.1%).

The Powder X-ray Diffraction Study. These data revealed three broad peaks ($2\theta \approx 12, 25, 37^\circ$) and practically no sharp peaks, implying the X-ray amorphism, possibly with a loose layered structure (Figure 3). No crystallization was observed upon long-term storage (up to one month) of the PAB samples.

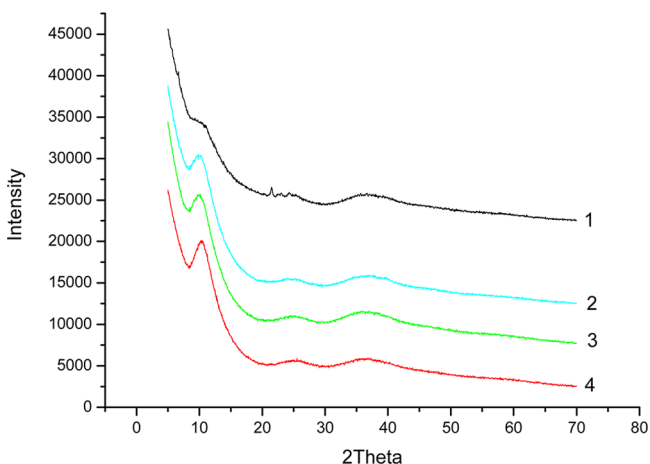


Figure 3. XRD patterns for PAB 1 samples of the empirical formula $\text{Pt}(\text{OOCMe})_{2.5}$ with different storage time: 1—as-prepared sample; 2—after 10 d; 3—after 30 d; 4—after three months of storage in air.

Scanning Electron Microscopy and Transmission Electron Microscopy Studies. In agreement with XRD data, SEM data (Figure 4) showed no well-formed crystalline particles. Secondary electron detectors (InLens and SE2) were used to obtain images in topographic contrast, and back-scattered electron detectors (ESB) were used to reveal the compositional contrast. The latter means that in the SEM image regions of the sample having different chemical composition (roughly, average atomic weight) are of different brightness: less average atomic weight is indicated by the darker the corresponding region. Images taken using ESB detector

(40 000 \times) revealed no compositional contrast, thus testifying to the homogeneity of PAB samples.

Similar irregular particles were also observed at the TEM micrographs (Figure 5a), while the HRTEM image revealed very small particles (ca. 50 Å) with distinct lattice fringes (Figure 5b).

Magnetic Susceptibility. Some mixed-valent paramagnetic platinum blue complexes are known.^{20,21} Our magnetic susceptibility measurements showed the antiferromagnetic behavior of as-prepared Pt blue samples (Figure 6).

The magnetic susceptibility decreases in time, and the PAB 1 samples become diamagnetic after storage for 30–40 d at room temperature. This observation is in accordance with the earlier found instability in time of the paramagnetic mixed-valent Pt blue complexes derived from 1-methylhydantoin and 5-methyl-2-pyrrolidinone.²⁶

Extended X-ray Absorption Fine Structure Spectra Study. Experimental data k^2 -weighted $\chi(k)$ versus k for the as-prepared and aged PAB1 samples (Figure 7a) showed high-quality spectra suitable for analysis in a wide wavenumber interval. This observation is supported by the Fourier transform in the 2.5–17.0 Å⁻¹ wavenumber interval (Figure 7b).

To obtain quantitative data, the calculation for $k^2\chi(k)$ was performed in the 4.0–12.6 Å⁻¹ interval, to eliminate the effect of multiple wave scattering at small photoelectron energies and to improve the signal/noise ratio at high photoelectron energies. The resulting Fourier transforms for the same PAB samples in the 4.0–12.6 Å⁻¹ interval (Figure 8) show that the main peaks are invariable in the positions and only slightly change the intensities.

The spectra were simulated with various molecular models, both containing and not containing long platinum–ligand distances. The best fit was found for the model with one Pt–O and two Pt–Pt distances within 4 Å (Figure 8, Table 1). The models with longer interatomic distances gave overestimated coordination numbers (N) for these distances, seemingly because of a high contribution of the multiple photoelectron scattering. Data in Table 1 show that the quality of modeling (R factor) is better for the aged PAB 1 sample, whereas the R factor for the as-prepared sample is higher seemingly because of a lower structure ordering and multiple photoelectron scattering.

Density Functional Theory Modeling. The simplest molecular units for modeling the PAB structure, taking into account the magnetic properties of PAB, are the binuclear odd-electron molecule $\text{Pt}(\mu\text{-OOCMe})_4\text{PtOOCMe}$ (A), bis-lantern (B–D), and triangle (E–G) structures (Figure 9).

The DFT-optimized geometry of this molecule reasonably reproduces the two shortest interatomic distances found by EXAFS (Pt–Pt ca. 2.50 Å and Pt–O_{br} ca. 2.00 Å). However, the longer distances do not fit the EXAFS data (Table 2). Assembling the lantern molecules 1 by “face–face” twinning (Figure 9, structure B) analogously to the known crystalline structures,^{9–11} and “face–tail” twinning through acetate (structure C) or OH bridge (structure D), does not improve the DFT–EXAFS agreement (cf. Tables 1 and 2). The triangle-based structures E–G gave no better agreement with EXAFS data; in particular, no short Pt–Pt distance ca. 2.50 Å was found in these structures (Figure 9, Table 2). This result suggests that PAB 1 has a more complicated structure, which we further portrayed with the MM+ modeling.

Molecular Mechanics Modeling. This method gave better agreement with EXAFS data. The fidelity criterion in

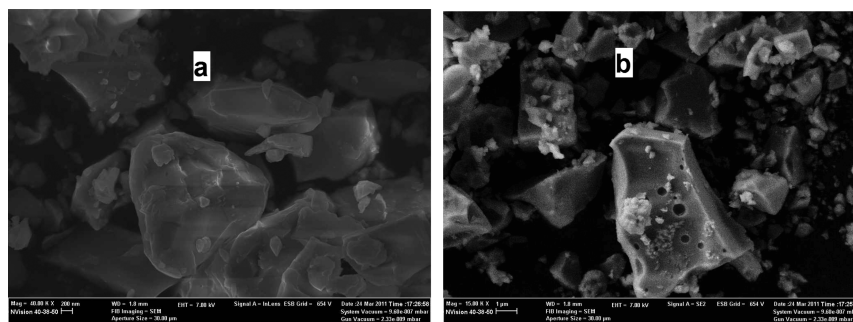


Figure 4. SEM micrographs of PAB 1 sample prepared by Protocol 1: (a) taken using an InLens detector (magnification 40 000 \times) and (b) taken using an SE2 detector (magnification 15 000 \times).

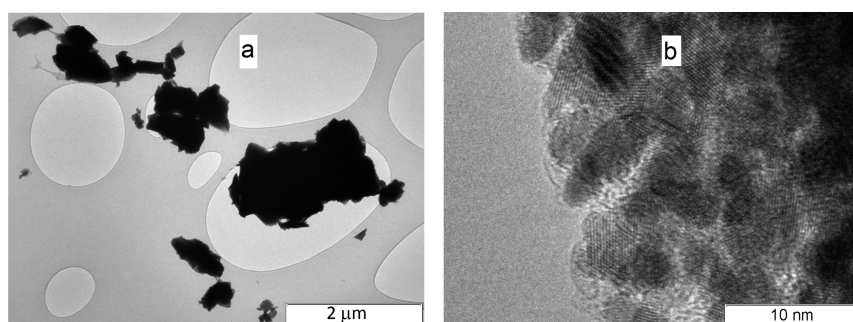


Figure 5. TEM (a) and HRTEM (b) micrographs of PAB 1 sample prepared by Protocol 1.

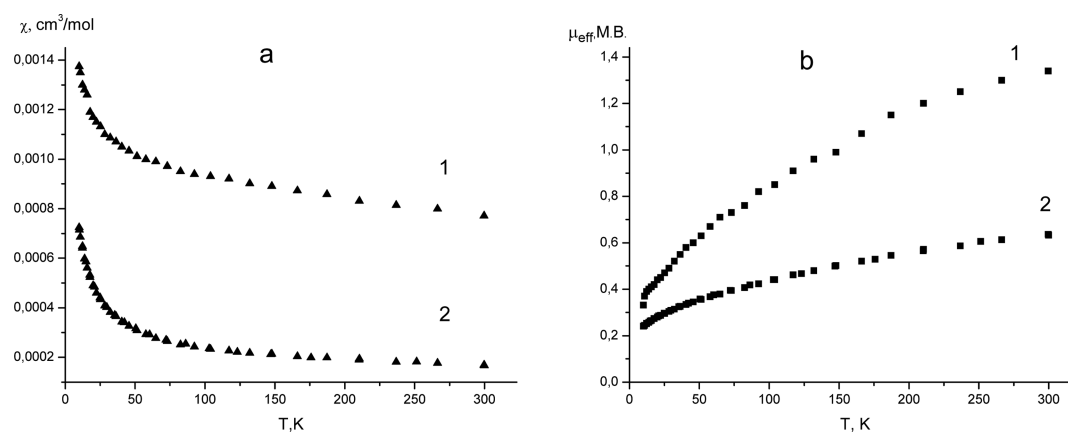


Figure 6. Magnetic susceptibility data for the as-prepared (1) and stored for 10 d (2) PAB 1 samples measured in the 4–300 K temperature interval: (a) molar magnetic susceptibility per $\text{Pt}(\text{OOCCH}_3)_2$ formula unit; (b) magnetic moment calculated for Pt atom.

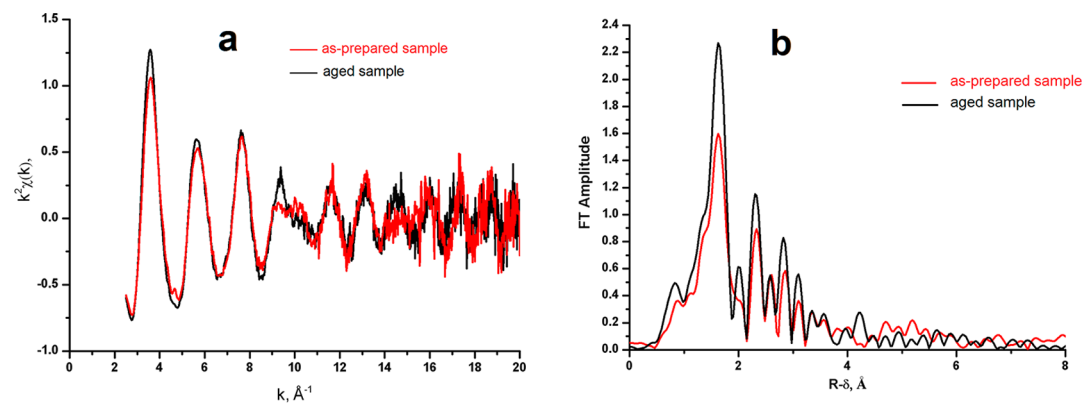


Figure 7. PtL_3 absorption spectra of as-prepared and aged PAB 1 samples: (a) oscillation part and (b) Fourier transform amplitude of $k^2\chi(k)$ in the wavenumber interval of 2.5–17.0 \AA^{-1} .

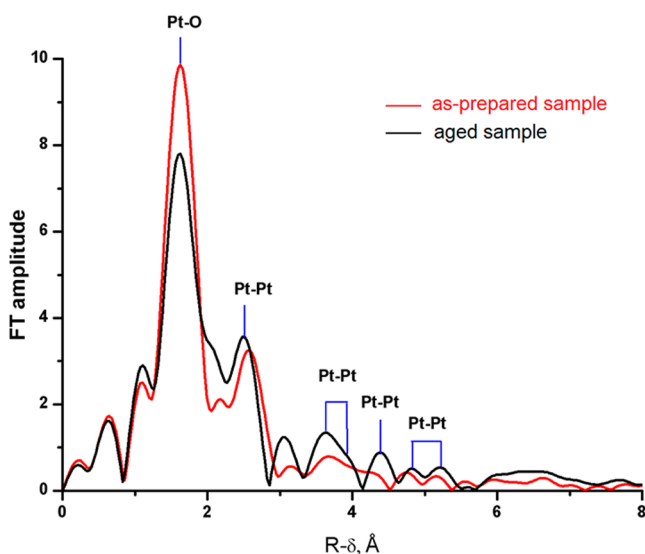


Figure 8. Fourier transforms of $k^3\chi(k)$ PtL_3 spectra for the as-prepared and aged PAB 1 samples in the $4.05\text{--}12.6 \text{ \AA}^{-1}$ interval.

Table 1. Results of Modeling the EXAFS Data for the Pt Surrounding of the As-Prepared and Aged PAB 1 Samples

interatomic distance	$R, \text{ \AA}$	N	$\sigma^2, \text{ \AA}^2$	$\Delta E_0, \text{ eV}$	R factor, %
As-Prepared PAB 1 Sample					
Pt–O	2.00	4.0	0.007	10.5	21.6
Pt–Pt	2.49	1.7	0.006		
Pt–Pt	3.81	1.0	0.006		
Aged PAB 1 Sample					
Pt–O	1.98	3.4	0.004	7.5	13.8
Pt–Pt	2.52	3.5	0.011		
Pt–Pt	3.81	2.2	0.013		

the calculations was the agreement of the calculated interatomic distance/coordination number N with those of the EXAFS and Pt/OOCMe elemental analysis data (see Table 3). When the MM+ calculation gave several close values of interatomic distances within 0.1 \AA , they were averaged to compare with EXAFS data. The shortest calculated distances, Pt–O and Pt–Pt, correspond to the interatomic bonds in the primary cluster. The coordination numbers for these distances were taken as the fidelity criterion. The next distance, Pt–Pt (3.8 \AA), seemingly corresponds to the packing of the primary clusters. The longer distances were attributed to the coupling of the primary triangles. The validity of the triangle-based approach is supported by the fact that no Pt–Pt 3.8 \AA distances were found for the lantern-based structures, and the calculated coordination number N for the shortest Pt–Pt distance ($\sim 2.5 \text{ \AA}$) was 1, whereas the EXAFS data gave the N value for this distance of at least 2.

Hence, the agreement of the MM+ modeling with the experimental data was achieved only when the triangle platinum structures were used as primary clusters. A good MM+–EXAFS fit in the coordination numbers for the shortest Pt–Pt distance was observed for all models; however, the Pt–Pt distance below 4 \AA was found only for the tribridged-triangle structures. When at least one bridge was broken, the triangles moved apart, and this distance disappeared. Table 4 presents the results of MM+ modeling in the comparison of EXAFS data.

The EXAFS and magnetic susceptibility data for the as-prepared and aged PAB 1 samples are different. For this reason

we analyzed two model structures. In the first structure the triangles are connected by acetate bridges, while in the second model some acetate bridges are replaced with OH bridging groups. This structure is allowable within the observed accuracy of the elemental analysis data. The partial OAc–OH replacement noticeably changes the coordination number and the Pt–Pt distances between and within the triangles. A rather high R factor in the EXAFS modeling of the as-prepared PAB sample suggests the presence of OH bridging groups in its structure; however, the exact number and distribution within the model molecule are still unknown.

Structure of Crystalline Complexes 1–3. 1. $\text{Pt}^{\text{II}}(\text{dipy})(\text{OOCMe})_2 \times (\text{MeCOOH}) \times (\text{C}_6\text{H}_6)_{0.5}$ (**1**). The reaction of PAB 1 with 2,2'-dipyridine produced two crystalline platinum(II) dipyrindine complexes, and one of them (complex **1**) was structurally characterized with X-ray diffraction analysis. Compound **1** is a cocrystallization complex consisting of *syn*- and *anti*-isomers of platinum(II) dipyrindine acetate and the crystallization molecules of acetic acid and benzene [*syn*-Pt(dipy)(OOCMe)₂] × [*anti*-Pt(dipy)(OOCMe)₂] × 2 MeCOOH × C₆H₆ (Figure 10).

Platinum atoms in both components have a typical square-planar coordination of two N atoms of the dipyrindine molecules (*syn*-isomer: Pt–N 1.986(5), 1.997(5) Å; *anti*-isomer: Pt–N 1.982(5), 1.990(5) Å) and two O atoms of the terminal acetate ligands (*syn*-isomer: O···O 2.596 Å; *anti*-isomer: O···O 2.602 Å). The crystal unit also contains one benzene crystallization molecule and two acetic acid crystallization molecules, which form short H bonds with the O atoms of one acetate ligand (*syn*-isomer: Pt–O 2.003(4), 2.016(4) Å; *anti*-isomer: Pt–O 2.012(4), 2.019(5) Å).

2. $\text{Pt}^{\text{II}}(\mu\text{-OOCMe})_4\text{Co}^{\text{II}}(\text{OH}_2) \times \text{MeCOOH}$ (**2**). The reaction of PAB 2 with $\text{Co}(\text{OOCMe})_2 \times 4\text{H}_2\text{O}$ produced the crystalline complex $\text{Pt}(\mu\text{-OOCMe})_4\text{Co}(\text{OH}_2) \times \text{MeCOOH}$ (**2**) in a 46% yield. The Pt(II) and Co(II) atoms in **2** are spaced at a short nonbonding distance of 2.481(4) Å (Figure 11). The Pt(II) atom has a typical square-planar environment of four O atoms of four bridging acetate anions, connecting Pt(II) with the Co(II) atom. The Co(II) atom is in a distorted tetragonal-pyramidal environment, including the O atom of the axial H₂O molecule (Pt–O 2.007(7)–2.104(7) Å, Co–O 1.983(17)–2.082(17) Å, Co–O_w 2.239(16) Å). The crystal unit of **2** also contains the solvate molecule of acetic acid that forms short H bonds with one O atom of the bridging acetate ligand (O···O 2.72 Å) and an O atom of the coordinated H₂O molecule (O···O 2.58 Å), forming a linear one-dimensional polymer.

3. $\text{Pt}^{\text{III}}_2(\text{OOCMe})_4(\text{O}_3\text{SPhMe})_2$ (**3**). The molecule of complex **3** has a typical lantern structure of two platinum(III) atoms with a short Pt–Pt bond (2.4094(12) Å) bridged with four acetate groups (Pt–O 2.005(6)–2.020(6) Å) (Figure 12). The *p*-toluenesulfonic anions are covalently bound in the axial positions to Pt atoms (Pt–O(5) 2.121(7) Å, S–O(5) 1.507(7) Å, S–O 1.444(7)–1.452(8) Å, S–C 1.778(10) Å).

It is noteworthy that the acetate-bridged binuclear platinum(III) complexes are generally cationic.^{26,27} Unlike this, complex **3** and the molecular complex $\text{Pt}^{\text{III}}_2(\text{OOCMe})_4(\text{O}_3\text{SMe})_2$ ²⁵ contain the anions of moderately strong *p*-toluenesulfonic and methanesulfonic acids covalently bound to the Pt^{III} atom, whereas the analogous diplatinum(III) tetraacetate-bridged complexes [Pt₂(μ-OOCMe)₄(H₂O)₂]X₂ (X = ClO₄[−], CF₃SO₃[−], and NO₃[−]) containing stronger acid anions are cations with nucleophilic H₂O molecules bound at the axial position to the Pt atoms.²⁷

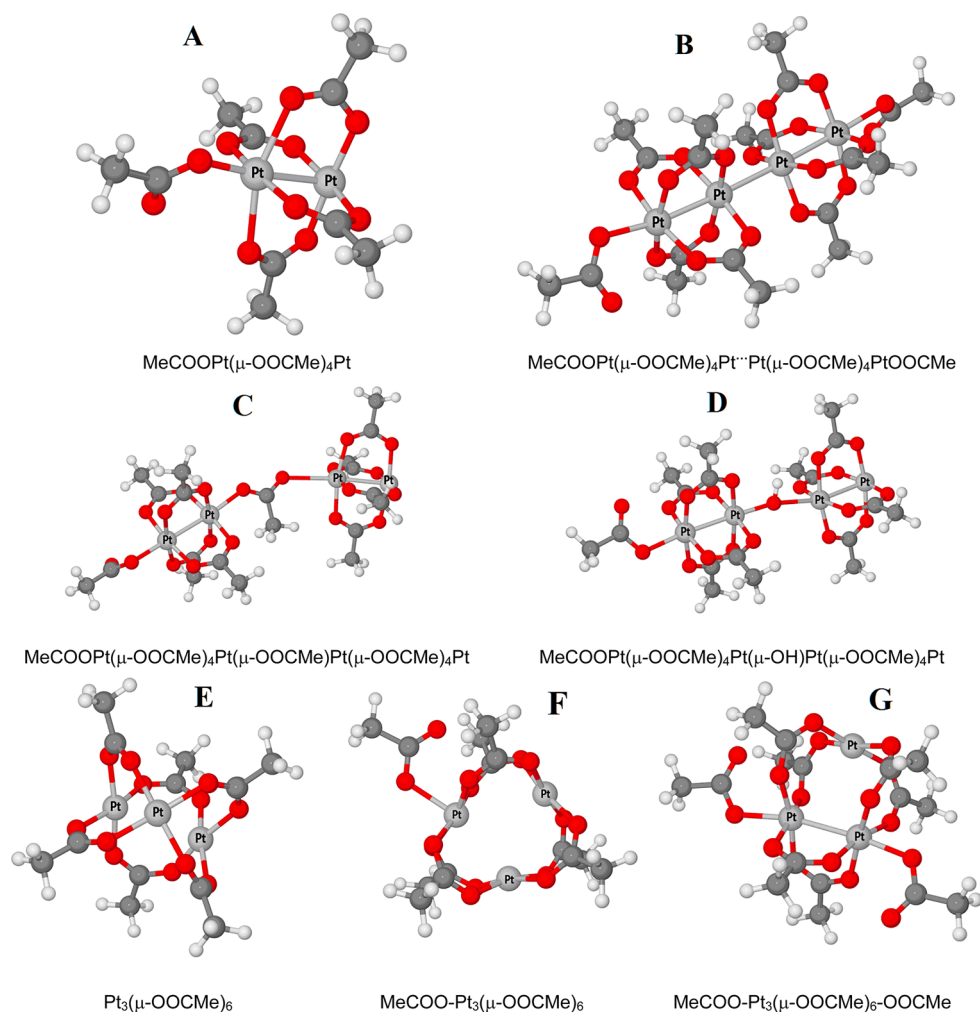


Figure 9. Equilibrium geometries of the lantern-based and triangle PAB structures.

Table 2. DFT-Calculated (M06/def2-SVP) Equilibrium Interatomic Distances (Å) in the Model Structures

structure	$R_1(\text{Pt-Pt})$	$R_2(\text{Pt-Pt})$	$R(\text{Pt-O}_{\text{equ}})$	$R(\text{Pt-O}_{\text{ax}})$
Triangle				
A	2.533		2.048; 2.373; 2.020	2.005
B	2.560	2.750	2.030–2.052	2.225
C	2.497; 2.681	6.887	2.028–2.068	2.116; 2.833
D	2.510; 2.673	4.640	2.026–2.068	2.064; 2.167
Lantern				
E	3.314	3.314	2.024	
F	3.048	3.382	2.018–2.028	2.244
G	2.665	3.489	2.013–2.022	2.143

CONCLUSIONS

The findings of this study provide some insight into the chemical nature of noncrystalline mixed-valent platinum acetate blues (PABs), which were repeatedly obtained as byproducts in the synthesis of platinum(II) acetate.^{6–8,11} At the first step we attempted to clarify whether PAB is a homogeneous material or a conglomerate of different species. The elemental analysis data for PAB samples prepared by protocols 1–3 are rather imperfect because of high dispersion of PAB samples, difficulties in their purification, and instability upon storage in a standard 1 mL vial in the air at ambient temperature and humidity. Nevertheless, the SEM, DTA-TG, and EXAFS data

gave certain evidence of the homogeneity of the PAB main body. Hence, the second step in our study was to search for the general structural features of this material. For this purpose, we attempted to find the equilibrium geometry of PAB structural fragments corresponding to the experimental data by DFT quantum chemical calculations. The DFT modeling of the lanternlike or triangle structures similar to the known crystalline platinum blues did not fit the EXAFS data, especially for the longer Pt–Pt distances, suggesting a more complicated structure or possibly a structure with C,O coordination of the acetate bridges similar to that found in the crystalline complex $\text{Cs}_3[\text{Pt}^{\text{III}}_2(\mu\text{-OCOMe})(\mu\text{-OOCMe})_2\text{Cl}_2]$.²⁸ Meanwhile, the MM+ analysis of possible structures showed at least two most probable structures, one for the as-prepared and another for aged PAB samples, which satisfactorily agree with the EXAFS data. Finally, the synthetic capabilities of the PAB were exemplified by the preparation and X-ray diffraction study of new homo- and heteronuclear platinum carboxylate complexes with the use of PAB as starting material. In these reactions, either platinum(II) or platinum(III) can be withdrawn from the mixed-valent PAB, depending on the reagent and solvent.

EXPERIMENTAL SECTION

Materials. Hexachloroplatinic(IV) acid $\text{H}_2[\text{PtCl}_6] \times 6\text{H}_2\text{O}$, potassium tetrachloroplatinate $\text{K}_2[\text{PtCl}_4]$, platinum(II) bromide PtBr_2 (Sigma-Aldrich), 2,2'-dipyridine $\text{C}_{10}\text{H}_8\text{N}_2$ (Reanal, Hungary),

Table 3. Best MM–EXAFS Fit Structures of the As-Prepared and Aged PAB 1 Samples

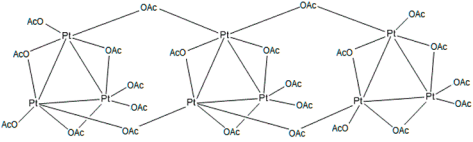
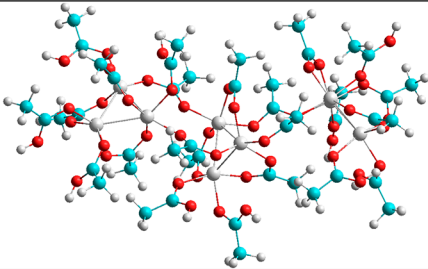
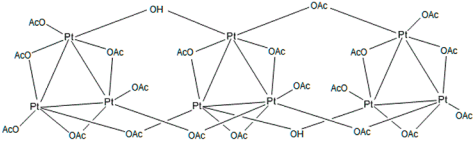
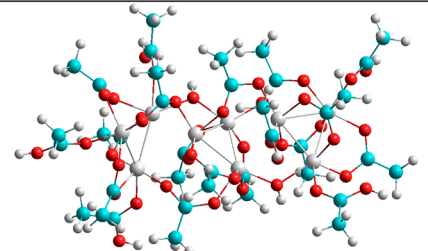
Structure type	Schematic view	Structure
Triple OAc-bridged triangle (as-prepared sample)	 <p style="text-align: center;">$\text{Pt}_9(\text{OOCMe})_{23}$</p>	
Triple OAc, OH-bridged triangle (aged sample)	 <p style="text-align: center;">$\text{Pt}_9(\text{OOCMe})_{21}(\text{OH})_2$</p>	

Table 4. Comparison of MM+ Modeling with EXAFS Data

distance	distances in optimized model	calculated		EXAFS	
		$R_{\text{ave.}}$	$N_{\text{ave.}}$	R	N
Triple OAc-Bridged Triangle $\text{Pt}_9(\text{OOCMe})_{23}$, As-Prepared PAB 1 Sample					
Pt–Pt	2.58, 2.59, 2.60, 2.60, 2.61, 2.62, 2.64, 2.65, 2.65	2.62	2.0	2.49	1.7
Pt–O	1.92–1.95	1.94	4.0	2.00	4.0
Pt–C _{inter.br}	2.78–2.90				
Pt–C _{outer.br}	2.92–3.04				
Pt–O	2.78–3.5				
Pt–C ₂	(3.28), 4.24–4.29				
Pt–Pt	3.62, ^a 3.91, ^a 3.76, ^a 3.84, ^a (4.69, ^a 4.84, ^a 4.94, ^a 5.13, ^a 5.17, ^a 5.30, ^a 5.63, ^a 5.66, ^a 5.73, ^a 5.93, ^a 6.59, ^a 6.90, ^a 6.94, ^a 7.10 ^a)	3.78	0.4	3.81	1.0
Triple OAc,OH-Bridged Triangle $\text{Pt}_9(\text{OOCMe})_{19}(\text{OH})_4$, Aged PAB 1 Sample					
Pt–Pt	2.57, 2.58, 2.59, 2.59, 2.61, 2.64, 2.66, 2.67, 2.67, 2.66	2.62	2.2	2.52	3.5
Pt–O	1.92–1.97, (1.90)	1.95	3.3	1.98	3.4
Pt–O _h	2.02, 2.03, 2.03, 2.07	2.03	0.7		
Pt–C _{inter.br}	2.62–2.93, 3.08, 3.09				
Pt–C _{outer.br}	2.77, 2.80, 2.92, 2.98, 2.98, 3.01, 3.07, 3.08				
Pt–C ₂	3.50–4.40				
Pt–Pt	3.01, ^a 3.15, ^a 3.39, ^a 3.51, ^a 3.59, ^a 3.62, ^a 3.94, ^a 4.79, ^a 4.83, ^a 4.86, ^a 4.87, ^a 4.90, ^a 5.01, ^a 5.64, ^a 5.66, ^a 5.82, ^a 6.39 ^a	3.46	0.8	3.81	2.3

^aPt–Pt distances outside the triangle.

cobalt(II) acetate $\text{Co}(\text{OOCMe})_2 \times 4\text{H}_2\text{O}$ (Sigma-Aldrich), *p*-toluenesulfonic acid (Sigma-Aldrich), KCl (Pharmkhim, Russia), formic acid (assay 90%, Pharmkhim, Russia), and solvents (glacial acetic acid, benzene, acetonitrile, all Pharmkhim, Russia) were used as received. Silver acetate $\text{Ag}(\text{OOCMe})$ was prepared by the reaction of silver nitrate AgNO_3 (Merck) with sodium acetate CH_3COONa (Pharmkhim, Russia).

Instrumentation. CHN elemental analyses were performed on an automated C,H,N(S)-analyzer EA-3000 (EuroVector). The platinum percentage was determined by ICP–AES on an atomic emission spectrometer IRIS Advantage (Thermo Jarrell Ash, USA). UV–vis spectra of solutions were recorded on a Varian Cary50 instrument. ATR spectra of solid samples were recorded on a Nicolet Nexus spectrometer with a Pike micro-ATR accessory in the region of 4000–400 cm^{-1} .

Thermoanalytic Measurements. The thermal behavior was studied by differential scanning calorimetry (DSC) and thermogravimetric analysis (TGA). TGA was performed under an argon flow (Ar, > 99.998%; O₂, < 0.0002%; N₂, < 0.001%; water vapor, < 0.0003%;

CH₄, < 0.0001%) (20 mL/min) in alundum crucibles, on a NETZSCH TG 209 F1 instrument at a heating rate of 10 °C/min. The weights of the samples used in TG experiments were 0.5–3 mg. DSC studies were carried out under an argon flow on a NETZSCH DSC 204 F1 calorimeter in aluminum cells at a heating rate of 5 °C/min. The weights of the samples were 4–10 mg. The thermal analysis data were processed with the use of the NETZSCH Proteus Thermal Analysis software according to ISO 11357–1, ISO 11357–2, and ISO 11358.

X-ray Diffraction Studies. The XRD studies of PAB were carried out using a Siemens D-500 diffractometer with monochromatized Cu $K\alpha$ irradiation (graphite monochromator on reflected beam).

Electron Microscopy. *Scanning Electron Microscopy.* SEM images of the PAB samples were obtained on a Carl Zeiss NVision 40 workstation at 7 kV accelerating voltage using InLens and SE2 secondary electron detectors, as well as an ESB backscattered electron detector (at 1 kV acceleration voltage). Secondary electron (obtained using InLens and SE2 detectors) and backscattered electron images (obtained using ESB detector) were taken from the same spots, to

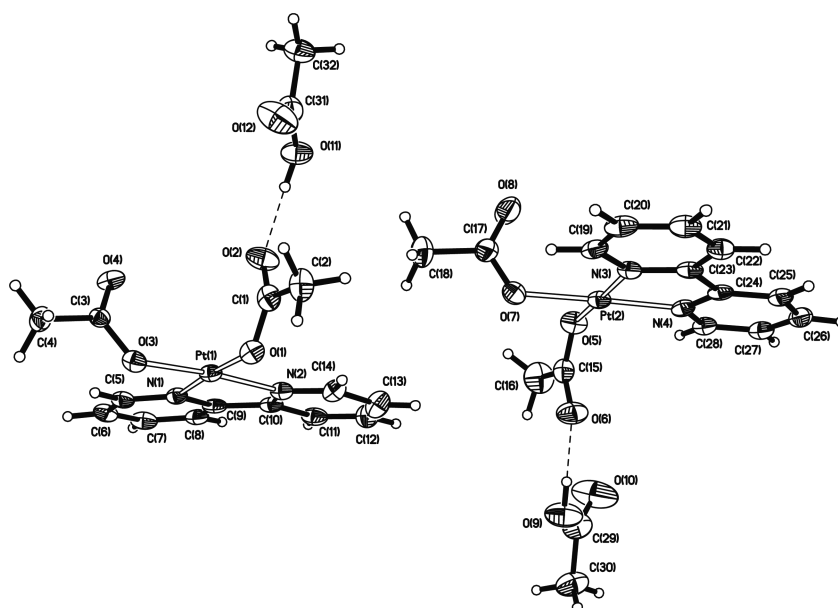


Figure 10. Molecular structure of the cocrystallization complex $[syn\text{-Pt(dipy)(OOCMe)}_2] \times [anti\text{-Pt(dipy)(OOCMe)}_2] \times 2\text{MeCOOH} \times \text{C}_6\text{H}_6$ (1) with thermal ellipsoids drawn at the 50% level (crystallization benzene molecule not shown).

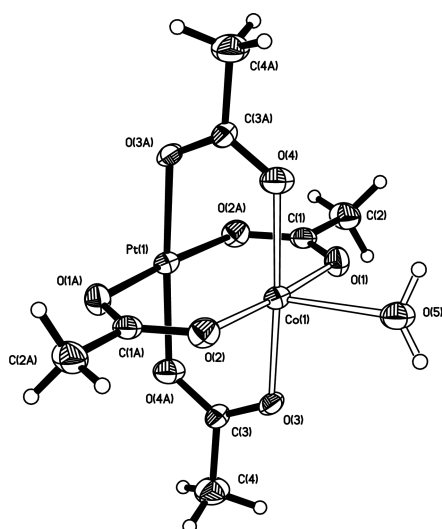


Figure 11. Molecular structure of the key component of the complex $\text{Pt}(\mu\text{-OOCMe})_4\text{Co}(\text{OH}_2) \times \text{MeCOOH}$ (2) with thermal ellipsoids at the 30% probability level (atoms Pt(1), Co(1), O(5) are disordered with a multiplicity of 0.5).

discriminate between topographic and compositional contrast. The SEM specimens were prepared by deposition of thin powder over an SEM holder.

High-Resolution Transmission Electron Microscopy. Detailed investigation of the PAB by high-resolution transmission electron microscopy (HRTEM) was carried out using a JEM-2010FX microscope with 1.4 Å line resolution. The specimens were ultrasonically dispersed in ethanol and dropped on a 200 mesh copper grid for HRTEM analysis.

Magnetic Susceptibility. These measurements were performed on a Quantum Design PPMS-9 (Physical Property Measurement System) in the temperature range of 1.8–300 K in a magnetic field of 5 kOe. The paramagnetic terms of the magnetic susceptibility χ were determined, taking into account the diamagnetic contribution evaluated from Pascal's constants. The temperature-dependent effective magnetic moment was calculated by the equation $\mu_{\text{eff}} =$

$[(3k/N\beta^2) \cdot \chi T]^{1/2} \approx (8\chi T)^{1/2}$, where N is Avogadro's number, k is the Boltzmann constant, and β is the Bohr magneton.

X-ray Structure Determination. Single-crystal XRD experiments were carried out on a Bruker SMART APEX II diffractometer with a CCD area detector (graphite monochromator, Mo $K\alpha$ radiation, $\lambda = 0.71073$ Å, ω scans). The semiempirical method SADABS²⁹ was applied for the absorption correction. The structures were solved by direct methods and refined by the full-matrix least-squares technique against F^2 with the anisotropic displacement parameters for all non-hydrogen atoms. All the hydrogen atoms in the complexes were placed geometrically and were included in the structure factors calculation in the riding motion approximation. All the data reduction and further calculations were performed using the SAINT³⁰ and SHELXTL-97³¹ program packages. Crystallographic parameters are given in the Supporting Information.

Extended X-ray Absorption Fine Structure Spectra. The spectra of the L_3 -edge platinum absorption were recorded by a standard procedure³² at the EXAFS station of the Siberian Synchrotron Radiation Center (Novosibirsk), using a VEPP-3 storage ring with an electron energy of 2 GeV and an average current of 80 mA as an X-ray source. A silicon monocrystal cutoff along a (111) plane was used as a monochromator. EXAFS spectra were recorded under transmission mode with a step of 2.0 eV, using proportional chambers as detectors. The polypropylene cell thickness was chosen to achieve an absorption jump of $\Delta\mu_x = 0.8$ at the platinum L_3 -edge. The oscillation part $\chi(k)$ of the EXAFS spectrum was analyzed as $k^3\chi(k)$ in the wave numbers range of $k = 4.0\text{--}12.6$ Å⁻¹. The radial distribution function was constructed without Fourier filtration. We used the VIPER software to isolate an oscillating part of the absorption and to execute spectrum simulations.³³ The FEFF-7 software helped to obtain scattering parameters.³⁴

Quantum Chemical Modeling. All DFT calculations were performed using a GAMESS-US program.³⁵ The geometries were optimized with the hybrid M06 functional³⁶ and the def2-SVP basis set,³⁷ with convergence criteria of 5×10^{-5} Hartree/Å for the gradient. The vibrational frequencies were calculated for the binuclear structures only. The starting geometries were constructed using an Avogadro program^{38,39} to agree with the EXAFS data.

Molecular Mechanics Modeling. This modeling of PAB was performed with the use of the calculation procedure MM+ of the program package HyperChem Pro 8.05,⁴⁰ with the standard atom potentials of the modified scheme MM2 (1991).^{41–43} To calculate the key interatomic distances and angles in the model complexes, the

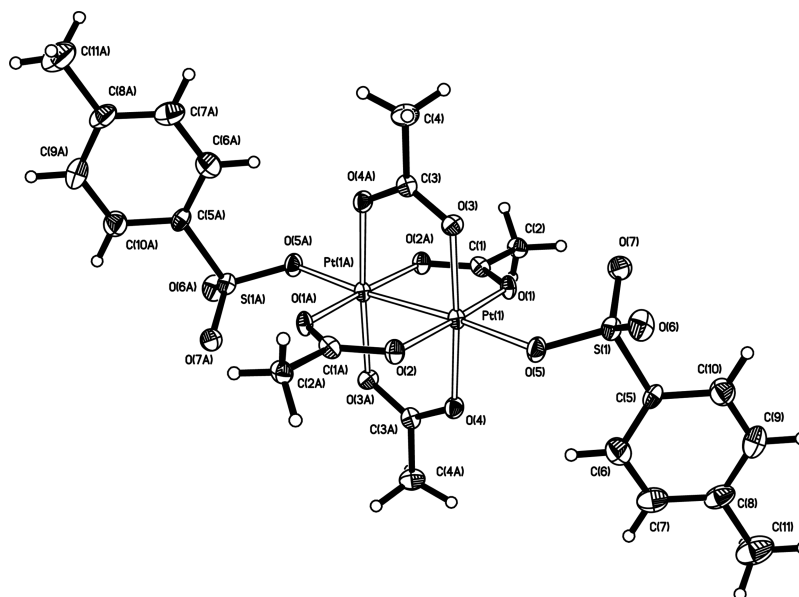


Figure 12. Molecular structure of the complex $\text{Pt}_2(\text{OOCMe})_4(\text{O}_3\text{SPhMe})_2$ (**3**) with thermal ellipsoids drawn at the 30% level.

structures were optimized by the steepest descents algorithm until the RMS-gradient 5×10^{-3} kcal/(Å·mol). Model structures are given in the Supporting Information.

Syntheses. PAB 1 (Protocol 1). A mixture of finely ground $\text{K}_2\text{Pt}(\text{OH})_6$ (1.00 g, 2.66 mmol), glacial acetic acid (50 mL), and formic acid (83.5 μL , assay 90%, 90.2 mg, 1.96 mmol) was stirred in a preheated (110 °C) oil bath until the temperature of the reaction mixture reached 95 °C (~12 min) and was further stirred at this temperature for 10 min. The reaction mixture was rapidly cooled to room temperature, and then a dark brown precipitate was separated by centrifugation from a violet-brown liquor, washed with cold glacial acetic acid (3×10 mL), and dissolved in 100 mL of hot glacial acetic acid until almost complete dissolution (110 °C, 90 min). The dark blue solution was filtered and evaporated to dryness on a rotary evaporator, and the dark blue residue was dried in a vacuum desiccator over KOH. Yield 446 mg, 49% based on Pt. Anal.: Found: Pt, 57.93; C, 16.47; H, 2.63. Calc. for $\text{Pt}_2\text{C}_{10}\text{O}_{10}\text{H}_{15}$, %: Pt, 56.92; C, 17.52; H, 2.21. ATR-FTIR spectrum (ν , cm^{-1}): 3409 w, 2936 w, 1720 w, 1625 w, 1554 m, 1404 s, 1341 s, 1305 s, 1041 m, 1015 m, 945 w, 696 w, 617 m, 577 m, 560 m, 552 w. The PAB 1 samples were aged in a standard 1 mL vial in the air at ambient temperature and humidity.

PAB 2 (Protocol 2). A solution of K_2PtCl_4 (830 mg, 2.00 mmol) in 20 mL of water was K-decated by passing it through a column with KU-2 cationite (H form), the eluent was concentrated to ~5 mL, supplemented with 10 mL of glacial acetic acid, and added to a warm (~50 °C) solution of CH_3COOAg (1.33 g, 8.01 mmol) in 80 mL of water. Then 85 mL of acetic acid was added, and the cloudy solution was stirred at 90 °C for 2 h under argon. The cooled reaction mass was centrifuged to separate AgCl from the dark-green solution. The dark-gray AgCl residue was washed with acetic acid (2×4 mL), and then the combined dark-green solution was supplemented with 30 mL of acetic acid and evaporated to dryness on a rotary evaporator at 50 °C. The greenish-black solid was dissolved in 5 mL of acetic acid, and the solution was centrifuged, evaporated to dryness on a rotary evaporator, and stored in a vacuum desiccator over KOH for 24 h. Yield 480 mg, 71% based on Pt. Anal.: Found: Pt, 57.77; C, 16.69; H, 2.50. Calc. for $\text{Pt}_2\text{C}_{10}\text{O}_{10}\text{H}_{15}$, %: Pt, 56.92; C, 17.52; H, 2.21. ATR-FTIR spectrum (ν , cm^{-1}): 3600–3380 br, 1630 m(sh), 1555 s, 1537 m, 1521 m(sh), 1349 m(sh), 1319 m(sh), 731 m, 715 m(sh), 692 m.

PAB 3 (Protocol 3). To a solution of platinum(II) bromide PtBr_2 (327 mg, 0.92 mmol) in 100 mL of boiling aqueous acetic acid (40 w/w) was added an aqueous solution of silver acetate AgOOCMe (292 mg, 1.76 mmol, 40 mL of boiling H_2O), which was stirred under reflux for 2 h in the dark. The resultant red-brown solution was filtered

successively through a fritted glass filter (F) and a Whatman 1001–055 paper filter to remove a black residue and evaporated to dryness on a rotary evaporator. The dry residue was dissolved in glacial acetic acid (20 mL), filtered through a fritted glass filter (F), evaporated to dryness, and dried over KOH in a vacuum desiccator. Yield 138.7 mg, 44% based on Pt. Anal.: Found: Pt, 56.04; C, 17.05; H, 2.10. Calc. for $\text{Pt}_2\text{C}_{10}\text{O}_{10}\text{H}_{15}$, %: Pt, 56.92; C, 17.52; H, 2.21.

$\text{Pt}^{\text{II}}(\text{dipy})(\text{OOCMe})_2$ (1). A mixture of PAB 1 of the empirical formula $\text{Pt}(\text{OOCMe})_{2.5}$ (137 mg, 0.40 mmol) and of 2,2'-dipyridine (62 mg, 0.40 mmol) in 20 mL of glacial acetic acid was stirred under reflux for 1 h. The reddish-brown solution was evaporated to dryness, and then the residue was dissolved in 20 mL of warm benzene and left in the air for crystallization at room temperature. A red fine-crystalline solid of the composition $\text{Pt}(\text{dipy})(\text{OOCMe})_2$ was precipitated in 12 h. Yield 148 mg, 78% based on Pt. Anal.: Found: Pt, 40.87; C, 35.77; H, 3.42; N, 5.71. Calc. for $\text{PtC}_{14}\text{O}_4\text{H}_{14}\text{N}_2$, %: Pt, 41.56; C, 35.82; H, 3.01; N, 5.97. ATR spectrum (ν , cm^{-1}): 3388 s, 3119 m, 3085 m, 2928 w, 1631m, 1605 s, 1470 w, 1452 m, 1425 w, 1367 s, 1313 s, 1248 w, 1162 w, 1019 m, 928 w, 895 w, 763 s, 719 s, 696 s, 613 s, 562 s. The red precipitate was filtered off, and the mother liquor was left for crystallization to give 85 mg (15% based on Pt) of the yellow crystals of $\text{Pt}(\text{dipy})(\text{OOCMe})_2 \times (\text{C}_6\text{H}_6)_{0.5} \times (\text{MeCOOH})$ (1) suitable for X-ray diffraction study. Anal: Found: Pt, 35.20, C, 38.37; H, 3.42; N, 5.51. Calc. for $\text{PtC}_{19}\text{H}_{21}\text{O}_6\text{N}_2$, %: Pt, 34.32; C, 40.13; H, 3.72; N, 4.93. ATR-FTIR spectrum (ν , cm^{-1}): 3358 s, 3113 m, 3080 m, 2928 w, 1712 w, 1640 m, 1605 s, 1468 w, 1452 m, 1368 s, 1314 s, 1308 s, 1247 m, 1164 w, 1164 w, 1064 w, 1047 w, 1027 m, 930 w, 905 w, 771 s, 721 m, 702 s, 613 s, 562 s. UV–vis spectrum of both complexes (acetic acid, λ_{max} nm): 310, 320, 360.

$\text{Pt}^{\text{II}}(\mu\text{-OOCMe})_4\text{Co}^{\text{II}}(\text{OH}_2)$ (2). PAB 3 of the empirical formula $\text{Pt}(\text{OOCMe})_{2.5}$ (100 mg, 0.29 mmol) and $\text{Co}(\text{OOCMe})_3 \times 4\text{H}_2\text{O}$ (73 mg, 0.29 mmol) was stirred in 4 mL of glacial acetic acid at 60 °C for 1 h. The initial dark green color changed to deep red in 15 min. The reaction solution was filtered and concentrated to 1 mL, and the 0.2 mL of benzene was added, before the solution was left for crystallization at room temperature. After 12 h the deep red crystals of $\text{Pt}(\text{OOCMe})_4\text{Co}(\text{OH}_2) \times \text{MeCOOH}$ were separated by decantation and dried under argon at room temperature. Yield 76 mg, 46% based on Pt. Anal.: Found: C, 21.46; H, 3.31. Calc. for $\text{PtCoC}_{10}\text{H}_{18}\text{O}_{11}$, %: C, 21.14; H, 3.19. ATR-FTIR spectrum (ν , cm^{-1}): 2926 w, 2914 w, 1709 s, 1623 vs, 1522 vs, 1460 s, 1402 vs, 1348 vs, 1334 m, 1269 m, 1051 w, 1026 m, 942 w, 889 w, 698 s, 626 s, 507 w, 456 w.

$Pt^{III}_2(OOCMe)_4(O_3SPHMe)_2$ (**3**). A mixture of PAB 1 of the empirical formula $Pt(OOCMe)_3$ (160 mg, 0.430 mmol), *p*-toluenesulfonic acid $p-CH_3C_6H_4SO_3H \times H_2O$ (84 mg, 0.44 mmol), and 10 mL of glacial acetic acid was stirred for 6 h at room temperature and remained at room temperature for 4 d, while the color of the solution changed from brown to dark green and a yellow fine-crystalline solid precipitated. The precipitate was separated by filtration and was washed successively with acetic acid, benzene, and diethyl ether. Yield 40 mg, 19% based on Pt. Anal.: Found: C, 26.93; H, 2.08; S, 6.49. Calc. for $Pt_2C_{22}O_{14}H_{26}S_2$, %: C 27.27; H, 2.71; S 6.61. The larger crystals of **3** that were suitable for X-ray diffraction study were obtained in the parallel synthetic run using 2 mL of glacial acetic acid as a solvent. ATR-FTIR spectrum (ν , cm^{-1}): 1565 m, 1415 s, 1349 w, 1273 s, 1151 s, 1121 w, 1095 m, 1034 w, 1021 w, 1008 w, 940 s, 813 m, 723 s, 708 w, 679 s, 636 w, 617 w, 581 m, 5560 s. These syntheses are also given in the Supporting Information.

■ ASSOCIATED CONTENT

■ Supporting Information

Synthesis protocols, DFT–MM+ optimized geometries, structures, and crystallographic parameters for complexes **1–3** are given. This material is available free of charge via the Internet at <http://pubs.acs.org>. The crystal structures were deposited at the Cambridge Crystallographic Data Centre and were allocated the deposition numbers CCDC 968031, 993748, 993749.

■ AUTHOR INFORMATION

Corresponding Author

*E-mail: wahr36@gmail.com. Phone: +7-985-955-48-65.

Notes

The authors declare no competing financial interest.

■ ACKNOWLEDGMENTS

The financial support provided by the Russian Foundation for Basic Research (Project Nos. 12-03-00917 and 12-03-31325), the Council on Grants at the President of the Russian Federation (Grant No. NSh-1712.2014.3), and the Foundation of the Russian Academy of Sciences (programs for Basic Research “Purposeful synthesis of inorganic substances and creation of related functional materials” and “Basic principles of technology of nanostructures and nanomaterials”) is gratefully acknowledged.

■ REFERENCES

- (1) Sakai, K.; Takeshita, M.; Tanaka, Y.; Ue, T.; Yanagisawa, M.; Kosaka, M.; Tsubomura, T.; Ato, M.; Nakano, T. *J. Am. Chem. Soc.* **1998**, *120*, 11353–11363.
- (2) Umakoshi, K.; Kojima, T.; Kim, Y. H.; Onishi, M.; Nakao, Y.; Sakaki, S. *Chem.—Eur. J.* **2006**, *12*, 6521–6527.
- (3) Ohashi, M.; Yagyū, A.; Yamagata, T.; Mashima, K. *Chem. Commun.* **2007**, *29*, 3103–3105.
- (4) Carrondo, M.A.A.F.; de, C. T.; Skapski, A. C. *J. Chem. Soc., Chem. Commun.* **1976**, 410–411.
- (5) Yamaguchi, T.; Sasaki, Y.; Nagasawa, A.; Ito, T.; N. Koga, N.; Morokuma, K. *Inorg. Chem.* **1989**, *28*, 4311–4312.
- (6) Stephenson, T. A.; Morehouse, S. M.; Powell, A. R.; Heffer, J. P.; Wilkinson, G. *J. Chem. Soc.* **1965**, 3632–3640.
- (7) Davidson, J. M.; Triggs, C. *Chem. Ind. (Chichester, U.K.)* **1966**, 306.
- (8) Rudy, R. I.; Cherkashina, N. V.; Mazo, G. Ya.; Salyn', Ya. V.; Moiseev, I. I. *Izv. Akad. Nauk SSSR, Ser. Khim.* **1980**, *4*, 754 [*Bull. Acad. Sci. USSR, Div. Chem. Sci. (Engl. Transl.)* 510–513].
- (9) Wright, D. British Patent No. 1214552; Imperial Chemical Industries: London, U.K., 1970.
- (10) Kunkely, H.; Vogler, A. *Inorg. Chem. Commun.* **2000**, *3*, 594–596.
- (11) Basato, M.; Biffis, A.; Martinati, G.; Tubaro, C.; Venzo, A.; Ganis, P.; Benetollo, F. *Inorg. Chim. Acta* **2003**, *355*, 399–403.
- (12) Ramstad, T.; Woollins, J. D. *Transition Met. Chem.* **1985**, *10*, 153–155.
- (13) Hofmann, K. A.; Bugge, G. *Ber. Dtsch. Chem. Ges.* **1908**, *41*, 312–314.
- (14) Barton, J. K.; Caravana, C.; Lippard, S. J. *J. Am. Chem. Soc.* **1979**, *101*, 7269–7277.
- (15) Lippert, B.; Neugebauer, D. *Inorg. Chem.* **1982**, *21*, 451–452.
- (16) Ginsberg, A. P.; O'Halloran, T. V.; Fanwick, P. E.; Hollis, L. S.; Lippard, S. J. *J. Am. Chem. Soc.* **1984**, *106*, 5430–5439.
- (17) Matsumoto, K.; Sakai, K.; Nishio, K.; Tokisue, Y.; Reikichi Ito, R.; Nishide, T.; Shichi, Y. *J. Am. Chem. Soc.* **1992**, *114*, 8110–8118.
- (18) O'Halloran, T. V.; Roberts, M. M.; Lippard, S. J. *J. Am. Chem. Soc.* **1984**, *106*, 6427–6428.
- (19) Mascharak, P. K.; Williams, I. D.; Lippard, S. J. *J. Am. Chem. Soc.* **1984**, *106*, 6428–6429.
- (20) Gencheva, G.; Mitewa, M.; Bontchev, P. R. *Polyhedron* **1992**, *11*, 2357–2361.
- (21) Arrizabalaga, P.; Castan, P.; Geoffroy, M.; Laurent, J.-P. *Inorg. Chem.* **1985**, *24*, 3656–3660.
- (22) Bandoli, G.; Dolmella, A. P.; Intini, F. P.; Pacifico, C.; Natile, G. *Inorg. Chim. Acta* **2003**, *346*, 143–150.
- (23) Lippert, B. *Chimia* **2008**, *61*, 732.
- (24) Cherkashina, N. V.; Kozitsyna, N.Yu.; Aleksandrov, G. G.; Vargaftik, M. N.; Moiseev, I. I. *Mendeleev Commun.* **2002**, *12*, 49–50.
- (25) Cherkashina, N. V.; Nefedov, S. E.; Klyagina, A. P.; Markov, A. A.; Vargaftik, M. N.; Moiseev, I. I. *Inorg. Chem. Commun.* **2012**, *21*, 39–42.
- (26) Wilson, J. J.; Lippard, S. J. *Inorg. Chem.* **2012**, *51*, 9852–9864.
- (27) Appleton, T. G.; Byriel, K. A.; Garrett, J. M.; Hall, J. R.; Colin, H. L.; Kennard, C. H.; Mathieson, M. T.; Stranger, R. *Inorg. Chem.* **1995**, *34*, 5646–5655.
- (28) Yamaguchi, T.; Sasaki, Y.; Ito, T. *J. Am. Chem. Soc.* **1990**, *112*, 4038–4040.
- (29) Sheldrick, G. M. *SADABS*; Bruker AXS, Inc.: Madison, WI, 1997.
- (30) *SMART V5.051 and SAINT V5.00, Area detector control and integration software*; Bruker, AXS Inc.: Madison, WI, 1998.
- (31) Sheldrick, G. M. *SHELXTL-97. V5.10*; Bruker AXS, Inc.: Madison, WI, 1997.
- (32) Kochubey, D. I. *EXAFS Spectroscopy of Catalysts*; Nauka: Novosibirsk, 1992.
- (33) Klementev, K. V. *Nucl. Instrum. Methods Phys. Res., Sect. A* **2000**, *448*, 299–301.
- (34) Zabinsky, S. I.; Rehr, J. J.; Ankudinov, A.; Albers, R. C.; Eller, M. *J. Phys. Rev. B* **1995**, *52*, 2995–3009.
- (35) Schmidt, M. W.; Baldrige, K. K.; Boatz, J. A.; et al. *J. Comput. Chem.* **1993**, *14*, 1347–1363.
- (36) Zhao, Y.; Truhlar, D. *Theor. Chim. Acta* **2008**, *120*, 215–241.
- (37) Weigend, F.; Ahlrichs, R. *Phys. Chem. Chem. Phys.* **2005**, *7*, 3297–3305.
- (38) (1) Avogadro: an open-source molecular builder and visualization tool. Version 1.1.1. <http://avogadro.openmolecules.net/>.
- (39) Hanwell, M. D.; Curtis, D. E.; Lonie, D. C.; Vandermeersch, T.; Zurek, E.; Hutchison, G. R. *J. Cheminf.* **2012**, *4*, 17.
- (40) *HyperChem Computational Chemistry*; Hypercube, Inc.: Gainesville, FL, 2002.
- (41) Allinger, N. L. *J. Am. Chem. Soc.* **1977**, *99*, 8127.
- (42) Allinger, N. L.; Yuh, Y. H. *MM2, Program No. 395, Quantum Chemistry Program Exchange*; Indiana University: Bloomington, IN.
- (43) Burkert, U.; Allinger, N. L. *ACS Monogr.* **1982**, *177*.